Geometric description of chaos in two-degrees-of-freedom Hamiltonian systems

Monica Cerruti-Sola[1] and Marco Pettini[1,2]

[1]*Osservatorio Astrofisico di Arcetri, Largo E. Fermi 5, 50125 Firenze, Italy*

[2]*INFN, Sezione di Firenze, Italy*

This paper tackles Hamiltonian chaos by means of elementary tools of Riemannian geometry. The stability of dynamics, related to curvature properties of the configuration space manifold, is investigated through the Jacobi–Levi-Civita equation (JLC) for geodesic spread. The case of two-degrees-of-freedom Hamiltonians is considered in general and is applied to the Hénon-Heiles model. The detailed qualitative information provided by Poincaré sections are compared with the results of geometric investigation; a complete agreement is found. The solutions of the JLC equation are also in quantitative agreement with the solutions of the tangent dynamics equation. It is shown here that chaos in the Hénon-Heiles model stems from parametric instability due to positive curvature fluctuations along the geodesics (dynamical motions) of configuration space manifold. This mechanism is apparently the most relevant—and in many cases unique—source of chaoticity in physically meaningful Hamiltonians. Hence a major difference with the geometric description of chaos in abstract ergodic theory is found; chaotic Hamiltonian flows of physics have nothing to do with Anosov flows defined on negative curvature manifolds. Even in the case of fully developed Hamiltonian chaos, hyperbolicity is not necessarily involved. Finally, the paper deals with the problem of finding other criteria for the onset of chaos based on purely geometric tools and independently of the numerical knowledge of the trajectories.

I. INTRODUCTION

Motivated by the need for effective analytic tools to tackle Hamiltonian chaos, a differential geometric approach has recently been proposed and successfully applied to the study of large Hamiltonian systems [1–4]. This method combines well known theoretical facts [5] with numeric simulations, resulting in a very powerful approach that provides an explanation of the origin of Hamiltonian chaos and an effective method to quantify it.

The starting point of the method is that trajectories of a standard Newtonian system can be viewed as geodesics of a Riemannian manifold endowed with a suitable metric. The instability properties of geodesics (and hence of the mechanical trajectories) are related to curvature properties of the underlying manifold through the Jacobi–Levi-Civita (JLC) equation for the evolution of geodesic separation. In the cited works, due to the large number of degrees of freedom, only *approximate* versions of the JLC equation for geodesic spread have been used. A basic question has been left open by the previous works. We wonder whether the geometric framework provides a complete description of dynamical stability. *A priori*, the large number of degrees of freedom together with the mentioned approximations of the JLC equation could hide a possible inadequacy of the approach.

The present paper is intended to clarify this point. In particular it aims at (i) showing that the Riemannian approach also works properly for systems with few degrees of freedom; (ii) showing that the *exact* JLC equation conveys all the detailed information about order and chaos, obtained through Poincaré section or Lyapunov exponent analysis of phase space at different energies; (iii) showing

that chaos in the Hénon-Heiles model—chosen as a paradigmatic example—stems from parametric instability due to positive curvature fluctuations along the geodesics of the configuration space manifold; and (iv) hinting at additional criteria for the onset of chaos based on a purely geometric analysis.

In Sec. II we recall the basic definitions and concepts of the geometric formulation of Newtonian mechanics and of its stability problem, making use of the JLC equation for a generic two dimensional system. In Sec. III—with the aid of a numerical study of the Hénon-Heiles model—we show that geometry contains all the information about order and chaos. In Sec. IV a brief account is given about the use of the integral of the negative sectional curvature—using the Eisenhart metric—to provide another way of detecting the stochasticity threshold.

II. RIEMANNIAN FORMULATION OF NEWTONIAN DYNAMICS

Let us consider a dynamical system described by the Lagrangian function

$$L(\mathbf{q}, \dot{\mathbf{q}}) = \tfrac{1}{2} a_{ik}(\mathbf{q}) \dot{q}^i \dot{q}^k - V(\mathbf{q}) , \qquad (1)$$

or, equivalently, after the usual Legendre transform, by the Hamiltonian

$$H(\mathbf{p}, \mathbf{q}) = \tfrac{1}{2} a^{ik}(\mathbf{q}) p_i p_k + V(\mathbf{q}) , \qquad (2)$$

where the momenta are given by $p_i = a_{ik}(\mathbf{q}) \dot{q}^k$. The mechanical trajectories of such a system are geodesics of the configuration space manifold endowed with a proper Riemannian structure described by the metric tensor [5]

$$g_{ik}(\mathbf{q}) = 2[E - V(\mathbf{q})]a_{ik} \ . \tag{3}$$

This metric is known as the Jacobi metric, and is defined in the region of configuration space where $E > V(\mathbf{q})$. We denote such a manifold by (M, g_J).

In local coordinates, the geodesic equations on a Riemannian manifold are given by

$$\frac{d^2 q^i}{ds^2} + \Gamma^i_{jk} \frac{dq^j}{ds} \frac{dq^k}{ds} = 0 \ , \tag{4}$$

where s is the proper time, and Γ^i_{jk} are the Christoffel coefficients of the Levi-Civita connection associated with g_{ik}. By direct computation, using $g_{ik} = [E - V(\mathbf{q})]\delta_{ik}$, $\Gamma^i_{jk} = (1/2W)\delta^{im}(\partial_j W \delta_{km} + \partial_k W \delta_{mj} - \partial_m W \delta_{jk})$, and $ds^2 = 2W^2 dt^2$, it can be easily verified that the geodesic equations yield

$$\frac{d^2 q^i}{dt^2} = -\frac{\partial V}{\partial q^i} \ , \tag{5}$$

i.e., Newton's equations for the Lagrangian (1) in the standard case $a_{ik} = \delta_{ik}$.

A geometrical point of view about the dynamical stability properties of natural motions, described by Eq. (5), stems from a relationship between the stability of the geodesics of a Riemannian manifold and the curvature properties of the same manifold.

This link between stability and curvature is mathematically expressed by the Jacobi–Levi-Civita equation for geodesic spread [6]. It describes the evolution of a vector field $\mathbf{J}$ through which the separation between nearby geodesics can be measured. The JLC equation reads

$$\frac{\nabla^2 \mathbf{J}}{ds^2} + R(\mathbf{v}, \mathbf{J})\mathbf{v} = 0 \ , \tag{6}$$

where $R(\ ,\ )$ is the Riemann curvature tensor, ∇/ds is the covariant derivative along a geodesic, and $\mathbf{v} = d\mathbf{q}/ds$.

In the majority of systems of physical interest (i.e., described by standard Hamiltonians) the instability of nearby trajectories can be studied by means of this equation. Now a remark is necessary about the relationship between geodesics instability and chaos.

The two basic topological conditions for the onset of chaos in any deterministic dynamics are *stretching* and *folding* of volumes in phase space [7]. In the case of Hamiltonian chaos, these two conditions are fulfilled by the existence of homoclinic intersections [7,8].

In the Riemannian description of Hamiltonian chaos, *stretching* of nearby trajectories is provided by *instability*, and *folding* by not allowing the distance to grow indefinitely; that is, by *compactness*. In this way, the phase trajectories fold themselves and forget the initial conditions; their evolution becomes unpredictable in the long run. In the majority of systems of physical interest, the ambient manifold (M, g_J) is compact, and the instability of nearby trajectories can be studied by means of Eq. (6).

This is what we are going to do in the simplest nontrivial case: two-degrees-of-freedom Hamiltonian systems.

Let us begin by considering the general case, and by as-

suming for the Jacobi field $\mathbf{J}$ the following decomposition:

$$\mathbf{J}(s) = \sum_i \xi_i(s) \mathbf{e}_{(i)}(s) \ , \tag{7}$$

where $\{\mathbf{e}_{(1)} \dots \mathbf{e}_{(N)}\}$ is an orthonormal system of parallelly transported vectors. In this reference frame it is

$$\frac{\nabla^2 \mathbf{J}}{ds^2} = \sum_i \frac{d^2 \xi_i}{ds^2} \mathbf{e}_{(i)}(s) \ , \tag{8}$$

and the second term of (6) is

$$R(\mathbf{v}, \mathbf{J})\mathbf{v} = \sum_j \langle R(\mathbf{v}, \mathbf{J})\mathbf{v}, \mathbf{e}_{(j)} \rangle \mathbf{e}_{(j)} \tag{9}$$

$$= \sum_j \left\langle R\left[\mathbf{v}, \sum_i \xi_i \mathbf{e}_{(i)}\right]\mathbf{v}, \mathbf{e}_{(j)} \right\rangle \mathbf{e}_{(j)} \tag{10}$$

$$= \sum_{ij} \langle R(\mathbf{v}, \mathbf{e}_{(i)})\mathbf{v}, \mathbf{e}_{(j)} \rangle \xi_i \mathbf{e}_{(j)} \ , \tag{11}$$

so that Eq. (6) is finally rewritten as

$$\frac{d^2 \xi_j}{ds^2} + \sum_i Q_{ij} \xi_i = 0 \ , \tag{12}$$

where $Q_{ij} = \langle R(\mathbf{v}, \mathbf{e}_{(i)})\mathbf{v}, \mathbf{e}_{(j)} \rangle$. To tackle the exact JLC equation at large dimension is a hard task because of the very large number of independent components of the curvature tensor. This is the reason why in previous works—concerning many-dimensional systems—we used only approximate versions of (6). In order to perform a detailed comparison between the information given by the geometric approach and the phenomenology obtained by standard means, here we restrict ourselves to the two-dimensional case—corresponding to a two-degrees-of-freedom Hamiltonian. In this case the study of order and chaos benefits very much from the use of Poincaré surface sections, and the comparison can actually be detailed.

In two dimensions there is a simple choice for $\{\mathbf{e}_{(1)}, \mathbf{e}_{(2)}\}$. In fact, take $\mathbf{e}_{(1)} \perp \mathbf{v}$ and $\mathbf{e}_{(2)} \| \mathbf{v}$; then since $\mathbf{v}$ is parallelly transported by definition of the geodesic, $\mathbf{e}_{(2)}$ is parallelly transported too, and if $\mathbf{e}_{(1)} \perp \mathbf{e}_{(2)}$ then $\mathbf{e}_{(1)}$ is also parallelly transported. So let us explicitly write their components with respect to a local (static) reference frame as

$$\mathbf{e}_{(1)} = \left[\frac{-dq^2}{ds}, \frac{dq^1}{ds} \right] \ , \tag{13}$$

$$\mathbf{e}_{(2)} = \left[\frac{dq^1}{ds}, \frac{dq^2}{ds} \right] \ , \tag{14}$$

so that $g_{ij} e^i_{(\alpha)} e^j_{(\beta)} = \delta_{\alpha\beta}$, and Eq. (12) now becomes

$$\frac{d^2 \xi_1}{ds^2} + \xi_1 (R_{klmn} v^k e^l_{(1)} v^m e^n_{(1)})$$

$$+ \xi_2 (R_{klmn} v^k e^l_{(2)} v^m e^n_{(1)}) = 0 \ , \tag{15}$$

$$\frac{d^2\xi_2}{ds^2}+\xi_2(R_{klmn}v^k e^{\,l}_{(2)}v^m e^{\,n}_{(2)})$$

$$+\xi_1(R_{klmn}v^k e^{\,l}_{(1)}v^m e^{\,n}_{(2)})=0 \ , \quad (16)$$

and in synthetic notation

$$\frac{d^2\xi_1}{ds^2}+Q_{11}\xi_1+Q_{12}\xi_2=0 \ , \quad (17)$$

$$\frac{d^2\xi_2}{ds^2}+Q_{22}\xi_2+Q_{21}\xi_1=0 \ . \quad (18)$$

The components of the Riemann tensor are $R^i_{jlk}=\partial_l\Gamma^i_{jk}-\partial_k\Gamma^i_{jl}+\Gamma^m_{jk}\Gamma^i_{ml}-\Gamma^m_{jl}\Gamma^i_{mk}$; in two dimension the only nonvanishing component is R_{1212}, and computed for the Jacobi metric of configuration space reads as

$$R_{1212}=\frac{\Delta V(\mathbf{q})}{2}+\frac{[\nabla V(\mathbf{q})]^2}{2W} \ , \quad (19)$$

with $W=E-V(\mathbf{q})$; Δ and ∇ are the Euclidean Laplacian and gradient, respectively. Let us remember that $R_{2112}=-R_{1212}$, $R_{2121}=R_{1212}$, and $R_{1221}=-R_{1212}$. Using (14), (19) and $\dot{q}^i=dq^i/ds=v^i$, a straightforward calculation yields $Q_{12}=Q_{21}=Q_{22}=0$ and

$$Q_{11}=R_{1212}\dot{q}^1 e^{\,2}_{(1)}\dot{q}^1 e^{\,2}_{(1)}+R_{2112}\dot{q}^2 e^{\,1}_{(1)}\dot{q}^1 e^{\,2}_{(1)}+R_{2121}\dot{q}^2 e^{\,1}_{(1)}\dot{q}^2 e^{\,1}_{(1)}+R_{1221}\dot{q}^1 e^{\,2}_{(1)}\dot{q}^2 e^{\,1}_{(1)}$$

$$=R_{1212}(\dot{q}^1 e^{\,2}_{(1)}-\dot{q}^2 e^{\,1}_{(1)})^2$$

$$=\frac{1}{W^2}\left[\frac{\Delta V}{2}+\frac{(\nabla V)^2}{2W}\right] \ . \qquad\qquad (20)$$

Hence Eqs. (17) and (18) become

$$\frac{d^2\xi_1}{ds^2}+\tfrac{1}{2}\mathcal{R}\xi_1=0 \ , \quad (21)$$

$$\frac{d^2\xi_2}{ds^2}=0 \ , \quad (22)$$

where $\mathcal{R}$ denotes the scalar curvature of configuration space.

It is obvious that a negative scalar curvature yields an unstable solution of Eq. (21). This is the case of abstract geodesic flows of ergodic theory, which are defined on hyperbolic manifolds (more precisely, they are defined on the unitary tangent bundle of manifolds of everywhere negative curvature). However, in the case of physical geodesic flows, the scalar curvature derived from the Jacobi metric, $\mathcal{R}=\Delta V/W^2+(\nabla V)^2/W^3$, has little chance to be negative. In fact, in order to have $\mathcal{R}<0$, it is necessary, but not sufficient, that $\Delta V<0$, and this does not happen for the majority of physical potentials, which are binding in the large range and only locally may give $\Delta V<0$.

Hyperbolicity is not the only way to make unstable solutions of Eq. (21). If $\mathcal{R}(s)$ is not constant, the loss of stability of the geodesics can be also induced by parametric resonance. Let us briefly recall what parametric resonance is. If the parameters of a dynamical system vary periodically in time, then a stable solution can be made unstable even if it is stable for each value of the parameters; this is the case of a harmonic oscillator whose frequency is periodically modulated in time with a suitable period [9]. We have shown in previous papers [1–4] that this is the dominant mechanism of instability in several physical geodesic flows on high-dimensional manifolds. In Sec. III, we show that this is also the case for a typical two-degrees-of-freedom system.

Passing from the proper time s to the physical time t in Eqs. (21) and (22), we find

$$\frac{d^2\xi_1}{dt^2}-\frac{1}{W}\frac{dW}{dt}\frac{d\xi_1}{dt}+\left[\Delta V+\frac{(\nabla V)^2}{W}\right]\xi_1=0 \ , \quad (23)$$

$$\frac{d^2\xi_2}{dt^2}=0 \ . \quad (24)$$

Equation (24) tells us that the parallel component of geodesic separation does not accelerate, thus only the transversal component ξ_1 conveys information about the behavior of nearby geodesics; and Eq. (23) describes without approximation the stability properties of the dynamics of two-degrees-of-freedom Hamiltonians. It is a scalar equation whose solutions are obtained by numerical integration simultaneously with the integration of the dynamical system under investigation.

If the solution $\xi_1(t)$ computed along a given trajectory remains bounded or grows at most linearly with time, then this trajectory is stable. If $\xi_1(t)$ grows exponentially with time, then the trajectory is chaotic, i.e., unstable with respect to any variation—even arbitrarily small—of coordinates and momenta operated at any given point of it.

Unstable solutions of Eq. (23) are produced by a nontrivial interplay of the last two terms. In fact $-\dot{W}/W$ takes both positive and negative values, so that it acts alternatively as a damping or an antidamping. In order to clarify how this interplay works, we make the substitution [10]

$$Y(t)=\xi_1(t)\exp\left[-\tfrac{1}{2}\int dt \ \dot{W}/W\right]\equiv\frac{\xi_1(t)}{\sqrt{W}} \ , \quad (25)$$

that recasts Eq. (23) in the form of a Hill equation

$$\frac{d^2 Y}{dt^2} + \Omega(t) Y = 0 \ , \tag{26}$$

where

$$\Omega(t) = \left[\Delta V + \frac{(\nabla V)^2}{W} \right] - \frac{1}{4} \left[\frac{\dot{V}}{W} \right]^2 - \frac{1}{2} \frac{d}{dt} \left[\frac{\dot{V}}{W} \right]$$

$$= \left[\Delta V + \frac{3(\nabla V)^2}{2W} \right] - \frac{3}{4W^2} \left[\dot{q}_1 \frac{\partial V}{\partial q_1} + \dot{q}_2 \frac{\partial V}{\partial q_2} \right]^2$$

$$- \frac{1}{2W} \sum_{i,k} \frac{\partial^2 V}{\partial q_i \partial q_k} \dot{q}_i \dot{q}_k \ . \tag{27}$$

From Eq. (25) we have $\xi_1(t) = \sqrt{W} \, Y(t)$, therefore $\xi_1(t)$ has the same stable or unstable behavior of $Y(t)$ (the pre-factor $\sqrt{W}$ has only bounded oscillations).

The stability equation (26), together with Eq. (27), is of general use for two-degrees-of-freedom Hamiltonian systems.

III. HÉNON-HEILES MODEL

In order to understand if all the information about order and chaos of a Hamiltonian system can actually be retrieved in the Riemannian approach, we apply the previous analysis to a very simple two-degrees-of-freedom system. In this case, detailed information about the phase space structure can be obtained by means of the Poincaré surfaces of the section. Therefore, by studying the stability of the solutions of Eq. (26) along the trajectories originating in regular and chaotic regions, it is possible to obtain *qualitative* information about order and chaos. In addition, by computing the solutions of Eq.
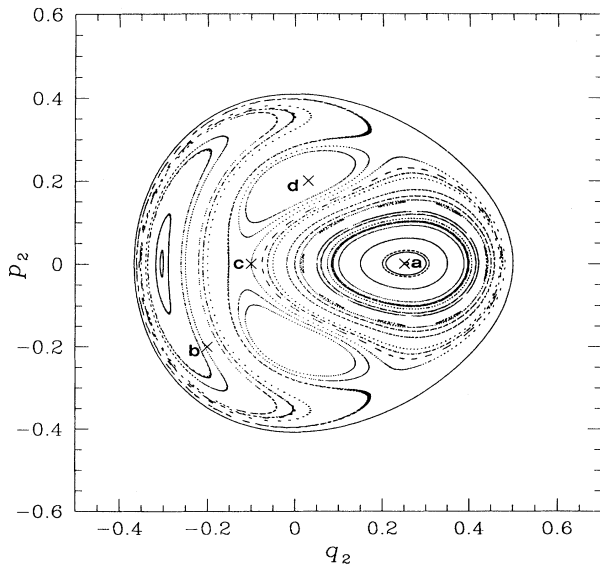
(26) together with the usual tangent dynamics equation, we can make a *quantitative* comparison between the geometric analysis and the traditional one.

We have chosen the Hénon-Heiles (HH) model, which, for historical reasons, is considered paradigmatic for the study of Hamiltonian chaos [11]. The HH Hamiltonian is written in the form

$$H = \tfrac{1}{2}(p_1^2 + p_2^2) + \tfrac{1}{2}(q_1^2 + q_2^2) + q_1^2 q_2 - \tfrac{1}{3} q_2^3 \ . \tag{28}$$

The equations of motion have been integrated by means of a Hammings modified predictor-corrector algorithm of
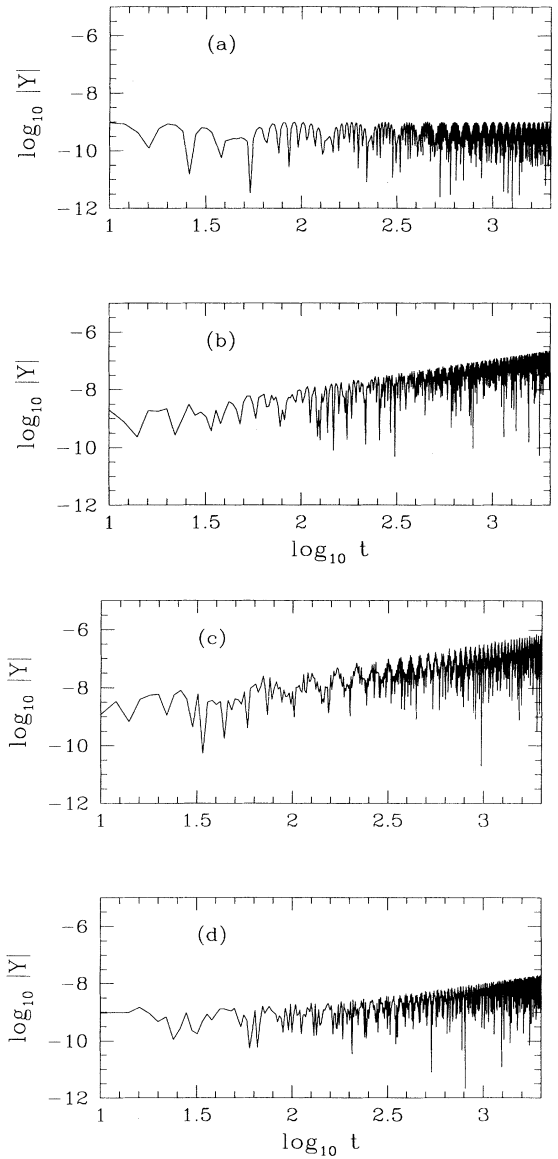

FIG. 2. The modulus $|Y(t)|$ of the solution of the stability equation (26) is plotted vs time for $E = 0.0833$. (a) The initial conditions (q_2, p_2) used for the integration are those at point a of Fig. 1. (b) At point b. (c) At point c. (d) At point d. Logarithms are decimal.

FIG. 1. Poincaré's surface of section for $E = 0.0833$ is shown. Crosses represent some initial conditions among those which have been chosen for the integration of Eq. (26).

fourth order. In order to perform a very accurate numerical integration of the dynamics, the integration time step is typically varied in the interval 10^{-4}–10^{-5}. Together with the equations of motion—and by means of the same algorithm—we have also integrated the JLC equation (6) in its equivalent form (26). We have considered three values of the total energy: $E = 0.0833$, 0.125, and 0.16667. Such a choice is only motivated by historical reasons. At each energy value we have chosen different initial conditions $[p_1(0), p_2(0), q_1(0),$ and $q_2(0)]$ for the dynamics, and we have kept $Y(0) = 10^{-9}$ and $\dot{Y}(0) = 0$ as initial conditions for Eq. (26).

As we want to make a qualitative comparison between the information provided by the Poincaré surfaces of section PSS and the solutions of Eq. (26), we choose the following initial conditions: $q_2(0)$ and $p_2(0)$, coordinates of the points located by the crosses marked on the PSS; $q_1(0) = 0$ (it defines the surface of section); $p_2(0)$ obtained from Eq. (28) [once E, $q_1(0)$, $q_2(0)$, and $p_1(0)$ are given] and assumed positive to meet the definition of the PSS.

We show in Fig. 1—marked by crosses—some representative points of the different disconnected regions that appear on the PSS at $E = 0.0833$. The solution of the stability equation (26) is reported for each point in Figs. 2(a)–2(d), all corresponding to the intersection of a regular trajectory with the considered plane of section; correspondingly the envelope of $Y(t)$ appears to be bounded or linearly growing in time. This is in agreement with the absence of chaoticity on the whole energy surface at $E = 0.0833$ (to be rigorous, a stochastic layer also always exists close to the separatrices in the presence of very weak perturbations, but its measure is extremely small below some energy threshold).

In Fig. 3 we show the PSS relative to $E = 0.125$; the crosses represent the four initial conditions for which $|Y(t)|$ is reported in Figs. 4(a)–4(d). The measure of the
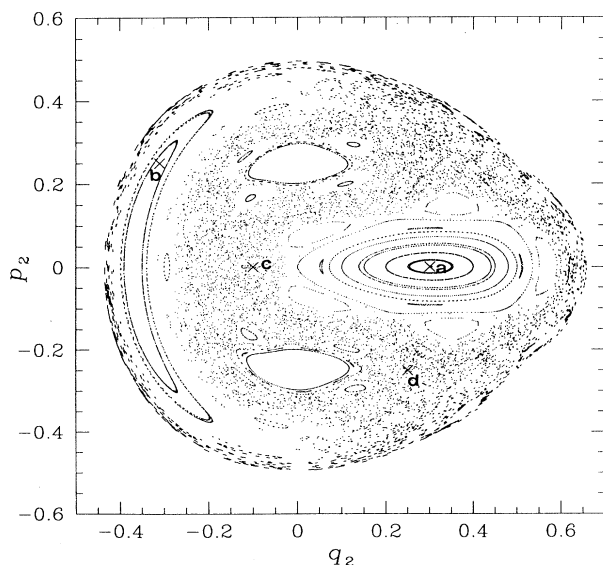
chaotic component of the phase space here is rather large; points c and d are representative of this chaotic part. The behavior of $|Y(t)|$ [Figs. 4(c) and 4(d)] is exponentially growing already at short times. At variance, points a and b, situated in regular islands, are characterized by solutions of the JLC equation which are bounded by a constant or linearly growing envelope in time [Figs. 4(a) and 4(b)].

The last case, at $E = 0.16667$, is the most chaotic one. The corresponding PSS is shown in Fig. 5, and again the
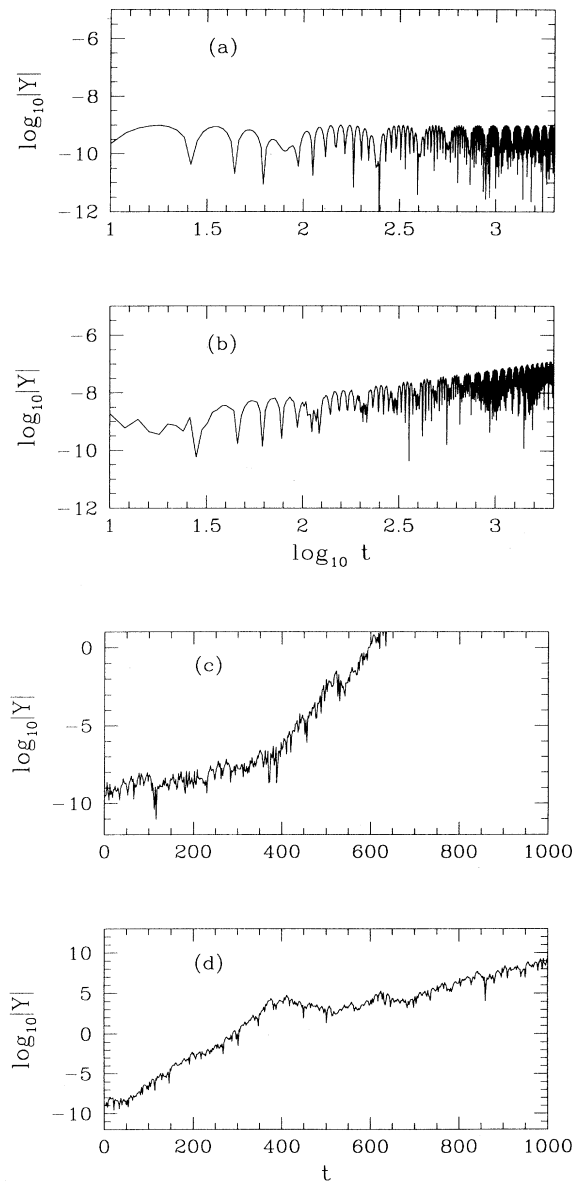

FIG. 3. The same as Fig. 1, but for $E = 0.125$.

FIG. 4. The behavior of $|Y(t)|$ solution of Eq. (26) is shown for $E = 0.125$. (a) The initial conditions (q_2, p_2) used for the integration are those at point a of Fig. 3. (b) At point b. (c) At point c. (d) At point d. Logarithms are decimal.
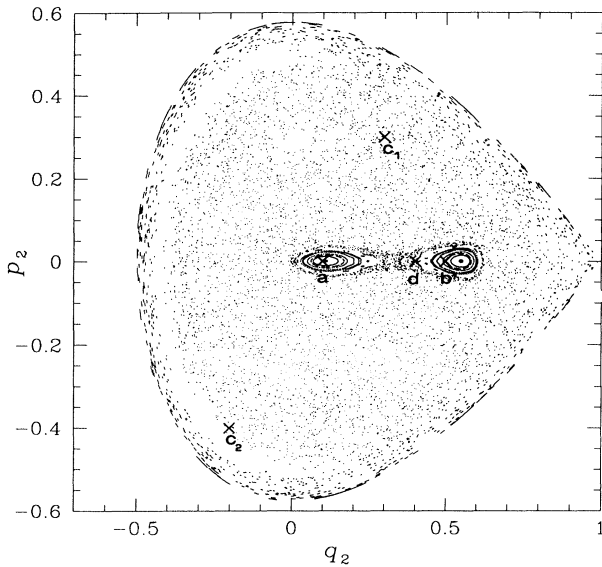
FIG. 5. The same as Figs. 1 and 3, but for $E = 0.1667$.

tuations of positive curvature.

We have just seen that the comparison between the detailed information given by PSS and from geometry reveals a complete *qualitative* agreement between the two. Now we can wonder if a *quantitative* agreement between standard and "geometrical" measures of the degree of chaoticity of the dynamics is also possible. For this reason, we have studied the conventional evolution equation for the vector field ξ of trajectory spread (tangent dynamics equation) at the energies and initial conditions of
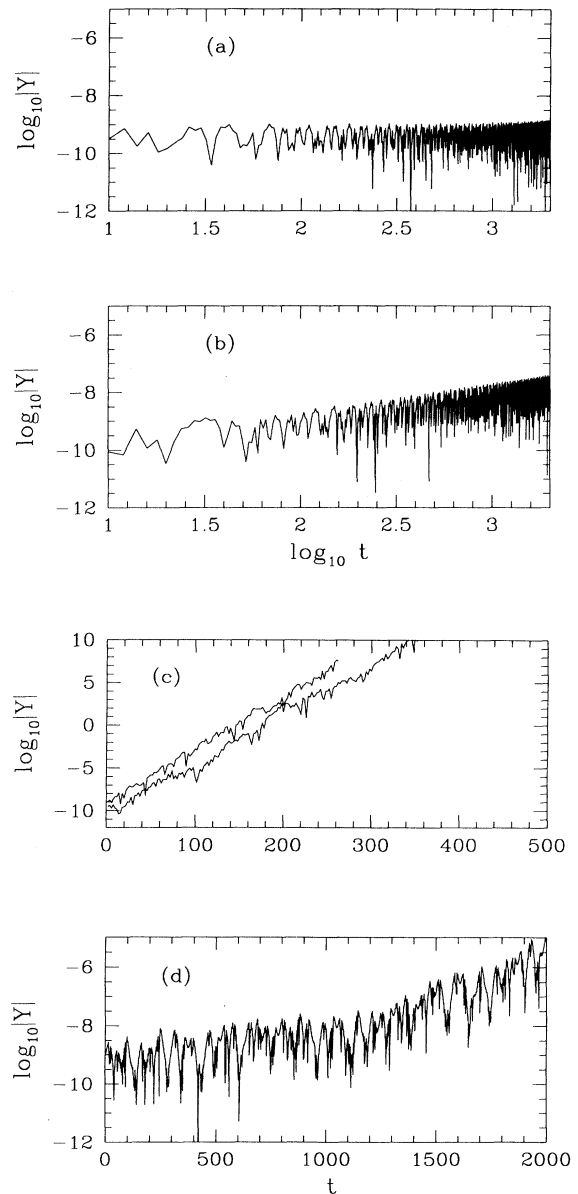
selected initial conditions are marked by five crosses. Only a few very small regular islands are concentrated in a small range of q_2 and p_2. Points a and b are just inside these regular regions. The behavior of $|Y(t)|$, computed for the trajectories stemming from these points, is constant or linearly growing [Figs. 6(a) and 6(b)] in time. It is worth noticing that the behavior of $|Y(t)|$ is peculiar at point d, just outside the regular island but not yet in the "chaotic sea"; in fact, $|Y(t)|$ displays a weak exponential growth which sets in at long times [Fig. 6(d)] and after a phase of even weaker growth. This provides a simple and clear illustration of the fact that the trajectories close to regular islands tend to stick to them. When the stability equation is integrated along the trajectories stemming from the points c_1 and c_2 that belong to the chaotic sea, $|Y(t)|$ grows exponentially in time [Fig. 6(c)]. Notice that the growth is now rather uniform in time for both solutions, and that their average growth rates are equal. We remark again that the pattern of $|Y(t)|$ provides a simple characterization of the degree of homogeneity of the chaotic part of the phase space.

It is worth mentioning that we extended our investigation to modified versions of the Hamiltonian (28) that are integrable [12] at any energy. Consistently, only bounded or linearly growing oscillations have been found for $|Y(t)|$. More details will be given in a forthcoming paper.

A trivial computation of R_{1212} of Eq. (19), and hence of the scalar curvature $\mathcal{R} = 2R_{1212}/W^2$, shows that both are *always positive* for the Hénon-Heiles model. Moreover, it is also a numerical fact that $\Omega(t)$, given by Eq. (27), is always positive, no matter whether it is computed along a regular or chaotic orbit. Therefore, in the geodesic flow defined by the Hénon-Heiles system, *chaos is due to the parametric instability of nearby geodesics induced by fluc-*

FIG. 6. The behavior of the solution of Eq. (26) is plotted for $E = 0.1667$. (a) The initial conditions (q_2, p_2) used for the integration are those at point a of Fig. 5. (b) At point b. (c) At points c_1 and c_2. (d) At point d. Logarithms are decimal.

position and velocity already considered for the integration of the stability equation (26).

The tangent dynamics equations, in the case of a standard Hamiltonian, have the form

$$\frac{d\xi_q^i}{dt} = \xi_p^i \ ,$$

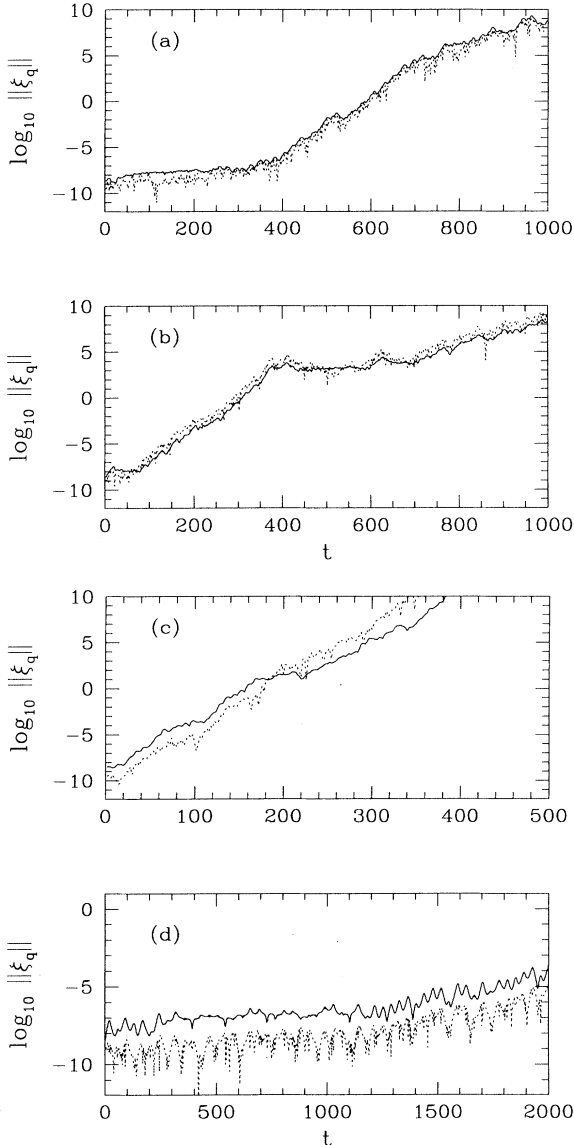$$\frac{d\xi_p^i}{dt} = -\frac{\partial^2 V}{\partial q_i \partial q^j}\xi_q^i \ ; \tag{29}$$

FIG. 7. (a) The evolution of the norm of ξ_q (solid line) is shown for $E = 0.125$ and initial conditions (q_2, p_2) at point c of Fig. 3. (b) Same as above, but at point d. (c) The norm of ξ_q (solid line) is shown for $E = 0.1667$ and initial conditions (q_2, p_2) at point c of Fig. 5. (d) The same, but at point d. As a comparison, the behavior of $|Y(t)|$, the solution of Hill's equation, is shown (dotted line) for the same values of E and the same initial conditions. Logarithms are decimal.

hence

$$\frac{d^2\xi_q^i}{dt^2} + \frac{\partial^2 V}{\partial q_i \partial q^j}\xi_q^j = 0, \quad i,j = 1,\dots,N \ , \tag{30}$$

whose solutions are to be compared with those of Eq. (26). In Figs. 7(a) and 7(b), the evolution of the norm $\|\xi_q\| = [(\xi_q^1)^2 + (\xi_q^2)^2]^{1/2}$ is plotted vs time at $E = 0.125$ and initial conditions of Figs. 4(c) and 4(d) (points c and d in Fig. 3). The dotted line represents, as a comparison, the behavior of $|Y(t)|$, as computed above. In Figs. 7(c) and 7(d), the evolution of the norm of ξ_q is shown vs time at $E = 0.16667$ and for initial conditions of Figs. 6(c) and 6(d) (points c and d in Fig. 5). Again, the dotted line shows the behavior of $|Y(t)|$. The fact that the solutions of the tangent dynamics equation give a very good *quantitative* agreement with the solution of the JLC equation is remarkable. At first sight this result is striking, inasmuch as Eqs. (26) and (30) appear very different from one another, and *a priori* there is no obvious reason for such a close resemblance of their solutions. However, this can be explained as follows. Equation (30) has a hidden geometric-differential origin in the sense that it can be derived from the JLC equation written for the Eisenhart metric g_E on the enlarged configuration space-time $M \times \mathbb{R}^2$ [2]. In Sec. IV, we shall briefly recall that the natural motions of a Newtonian system can be also seen as geodesics of $(M \times \mathbb{R}^2, g_E)$. Now, since the stability (instability) of natural motions is an intrinsic property, one has to find the same behavior of the solutions of the JLC equation, independently of the ambient manifold chosen to describe the motion. Hence it is no longer surprising that Eqs. (26) and (30) lead to the same result.

IV. TOWARD A GEOMETRIC STOCHASTICITY CRITERION

We have seen that all the information about order and chaos is concealed in the geometry of the configuration space manifold. The question naturally arises, of whether we can obtain some information about the global degree of chaoticity at different energies simply by measuring some geometric property of the ambient manifold. In other words, we wonder if it is possible to obtain this information by means of *static* computations, independently of the numerical integration of the dynamics.

It has recently been shown that this is actually possible when the number of degrees of freedom is high [1–3], whereas the two-degrees-of-freedom case is more delicate. This might appear to go against intuition, but the reasons are simple. Since parametric resonance is the dominant mechanism that causes chaos in physical Hamiltonians, in high-dimensional systems one can take advantage of the large number of degrees of freedom to make a Gaussian hypothesis about the statistics of curvature fluctuations along a geodesic. This approximation makes possible the analytic computation of the largest Lyapunov exponent independently of the dynamics [3], and hence an analytic computation of the transition energy from weak to strong chaos. In the case of two degrees of freedom, the arguments based on the central limit theorem [3] are

not applicable, and the statistics of curvature fluctuations along a geodesic cannot be modeled by a Gaussian process.

The Chirikov resonance overlap criterion and the Escande-Doveil renormalization method [8] are the only ways to describe the order-to-chaos transition in two-degrees-of-freedom systems. Both methods tackle the transition to chaos from the *indirect* point of view of the ordered trajectories, reducing the problem to the study of the loss of stability of the most robust *KAM* torus that separates the phase space into disjoint regions.

At variance, we want to tackle the transition to chaos *directly*, by studying the chaotic component of phase space. A difficulty immediately arises: from the point of view of parametric resonance, we should know the whole history of curvature fluctuations, and we could not get rid of the dynamics. On the contrary, we shall see in the following that an approach which uses an average geometric property of the ambient manifold related to the pointwise instability of the geodesics makes it possible to point out the transition from order to chaos (at least for the model under consideration).

Note that by simple algebraic manipulations of the JLC equation (6) one finds the evolution equation for the norm of the geodesic separation vector **J** in a form which is independent of the metric and valid at any dimension [2]:

$$\frac{1}{2}\frac{d^2\|\mathbf{J}\|^2}{ds^2}+K^{(2)}(\mathbf{J},\mathbf{v})\|\mathbf{J}\|^2-\left\|\left\|\frac{\nabla}{ds}\mathbf{J}\right\|\right\|^2=0\ , \tag{31}$$

where $K^{(2)}(\mathbf{J},\mathbf{v})$ is the sectional curvature given by

$$K^{(2)}(\mathbf{J},\mathbf{v})=R_{\mu\nu\eta\lambda}\frac{J^\mu}{\|\mathbf{J}\|}\frac{dq^\nu}{ds}\frac{J^\eta}{\|\mathbf{J}\|}\frac{dq^\lambda}{ds}\ , \tag{32}$$

and $\langle\mathbf{J},\mathbf{v}\rangle=0$. It is now evident from (31) that any point where $K^{(2)}<0$ is an unstable point. If along a geodesic the number of such points is on the average a linearly growing function of the proper time, then the whole geodesic is most probably unstable [13]. The same argument can be extended to the energy surface Σ_E: we assume that the existence of a positive measure of points of negative sectional curvature $K^{(2)}$ on Σ_E is a *sufficient* conditions for the existence of chaotic trajectories.

We remark that, after Eq. (31), the stability of the geodesics is controlled by $K^{(2)}$ rather than by $\mathcal{R}$. Only in the case of constant curvature manifolds does $K^{(2)}=\mathcal{R}/N(N-1)$.

Let us now focus on the two-degrees-of-freedom case. The ambient manifold (M,g_J) is now a two-dimensional space: scalar and Ricci curvatures coincide with the unique sectional curvature (the Gaussian curvature). On the other hand, it is well known that natural motions of a standard Hamiltonian system can be seen at the same time as geodesics of different ambient manifolds: configuration space with the Jacobi metric (M,g_J), configuration-space-time with the Eisenhart metric $(M\times\mathbb{R},\widetilde{g}_E)$ [14], enlarged configuration-space-time with another Eisenhart metric $(M\times\mathbb{R}^2,g_E)$ [14], and constant energy submanifold of the tangent bundle of

configuration space with Sasaki metric (TM,g_S,E) [15]. Although all descriptions must give the same results for what concerns the dynamical stability, *a priori* we can expect that more information is obtained using larger manifolds. For instance, if we associate a manifold with more than two dimensions to a given two-degrees-of-freedom system, then there is more than one sectional curvature. This also makes it possible to find $K^{(2)}<0$, where scalar and Ricci curvatures are positive. In fact, if $X_{(a)}$ are N orthonormal vectors on a manifold of dimension N, the Ricci curvature along $X_{(s)}$ is given by $K_R=\sum_{r=1}^N K^{(2)}(X_{(r)},X_{(s)})$. If K_R is positive, only the sum of the different sectional curvatures is constrained to be positive and not all the $K^{(2)}$. Therefore, looking for negative sectional curvatures *in an enlarged manifold* could provide a first step on the way of finding a stochasticity criterion for two-degrees-of-freedom systems.

One of the possible choices for a larger ambient manifold is the enlarged configuration-space-time $(M\times\mathbb{R}^2,g_E)$ equipped with the Eisenhart metric [14]. Let us briefly recall some major points concerning this.

The local coordinates of the enlarged configuration-space-time $(M\times\mathbb{R}^2,g_E)$ are $q^0,q^1,\ldots,q^i,\ldots,q^N,q^{N+1}$, where $(q^1,\ldots,q^N)\in M$, $q^0\in\mathbb{R}$ is the time coordinate and $q^{N+1}\in\mathbb{R}$ is an extra coordinate related to the action.

For standard Hamiltonian functions $H=T+V(\mathbf{q})$, the metric tensor g_E is defined in this coordinate system by

$$ds_E^2=(g_E)_{\mu\nu}dq^\mu dq^\nu$$

$$=a_{ij}dq^i dq^j-2V(\mathbf{q})(dq^0)^2+2dq^0 dq^{N+1}\ , \tag{33}$$

where $\mu,\nu=0,1,\ldots,N+1$, $i,j=1,\ldots,N$, and a_{ij} is the kinetic energy matrix. Among all the geodesics of this metric, those for which $ds_E^2=2C_1^2 dt^2$ are natural motions of the system. Consequently, $q^{N+1}(t)=C_1^2 t+C_2-\int_0^t L(\mathbf{q},\dot{\mathbf{q}})dt$. C_1 and C_2 are arbitrary constants.

If we assume that the energy matrix is diagonal, i.e., $a_{ij}=\delta_{ij}$, the only nonvanishing Christoffel coefficients are

$$\Gamma_{00}^i=\partial^i V,\quad \Gamma_{0i}^{N+1}=-\partial_i V\ , \tag{34}$$

and the geodesic equations (4) yield Newton equations of motion together with two other equations which are the differential versions of $q^0=t$ and $q^{N+1}(t)$ as defined above [1].

Another interesting characteristic of the Eisenhart metric is that the relevant geometric quantities, such as Riemann and Ricci tensors, have a very simple form, and the JLC equation (6) written for the manifold $(M\times\mathbb{R}^2,g_E)$ coincides with the tangent dynamics equation (30) (see [1,2]). The nonvanishing components of the Riemann tensor are $R_{0i0j}=\partial^2 V/\partial q^i\partial q^j$, so that for two-degrees-of-freedom Hamiltonians there are now three independent components instead of one. The sectional curvatures (32) have the following form (passing from proper time s to physical time t):

$$K^{(2)}(\mathbf{J},\mathbf{v})=R_{i0j0}\frac{J^i}{\|\mathbf{J}\|}\frac{dq^0}{dt}\frac{J^j}{\|\mathbf{J}\|}\frac{dq^0}{dt}$$

$$=\frac{1}{\|\mathbf{J}\|^2}\left[\frac{\partial^2 V}{\partial q_1^2}J_1^2+\frac{\partial^2 V}{\partial q_2^2}J_2^2+2\frac{\partial^2 V}{\partial q_1\partial q_2}J_1J_2\right].$$

$$(35)$$

This quantity depends on $\mathbf{q}(t)$ and $\mathbf{J}(t)$, and now can take also negative values where the Ricci curvature is positive [with the metric (33) the scalar curvature is always zero]. Instead of searching for these negative values along a geodesic, we look for them on the constant energy surface Σ_E by choosing arbitrary pairs of vectors $\mathbf{v}$ and $\mathbf{J}$ such that $\langle\mathbf{J},\mathbf{v}\rangle=0$. A simple possibility is $\mathbf{J}=(J_0=0,J_1=\dot{q}_2,$ $J_2=-\dot{q}_1,\ J_3=0)$ and $\mathbf{v}=(v_0\equiv 1,\ v_1=\dot{q}_1,\ v_2=\dot{q}_2,$ $v_3=\dot{q}_3)$, where q_3 is the extra coordinate; the choice of v_3 and J_3 is irrelevant because $g_{33}=0$. The sectional curvature relative to any such pair of vectors is given by

$$K^{(2)}(\dot{\mathbf{q}},\mathbf{q})=\frac{1}{2W}\left[\frac{\partial^2 V}{\partial q_1^2}\dot{q}_2^2+\frac{\partial^2 V}{\partial q_2^2}\dot{q}_1^2-2\frac{\partial^2 V}{\partial q_1\partial q_2}\dot{q}_1\dot{q}_2\right],$$

$$(36)$$

that is now computable—independently of the dynamics—on the constant energy surface Σ_E. By using $\mathbf{p}=\dot{\mathbf{q}}$, the integral $\langle K_{(-)}^{(2)}\rangle$ of the negative values assumed by the sectional curvature is

$$\langle K_{(-)}^{(2)}\rangle=\frac{1}{A(\Sigma_E)}\int_{\Sigma_E}d\sigma_E K_{(-)}^{(2)}$$

$$=\frac{1}{A(\Sigma_E)}\int d\mathbf{p}\,d\mathbf{q}\,\delta[H(\mathbf{p},\mathbf{q})-E]$$

$$\times\Theta[-K^{(2)}]K^{(2)}(\mathbf{p},\mathbf{q}),\qquad(37)$$

where the area $A(\Sigma_E)=\int_{\Sigma_E}d\sigma_E=\int d\mathbf{p}\,d\mathbf{q}\,\delta[H(\mathbf{p},\mathbf{q})-E]$, and Θ is the step function $[\Theta(x)=0$ if $x<0$, and $\Theta(x)=1$ if $x\geq 0]$.

This quantity has been computed at different energy values E and compared with the results of Ref. [11]; here the authors have shown that the transition from order to chaos can be quantitatively proved by measuring on a surface of section the ratio μ between the area covered by the regular trajectories and the total area accessible to the motions.

One can see from Fig. 8 (open circles) that, for low energies, the whole area is practically covered by regular curves ($\mu=1$); as the energy is increased, the ratio μ begins to decrease below 1, and drops rapidly to very low values. Beyond $E=\frac{1}{6}$, the accessible area becomes infinite (the equipotential lines are open), the motions are unbound, and the curve cannot be continued. If we put on the same plot the integral of the negative sectional curvature computed according to Eq. (37) and modified
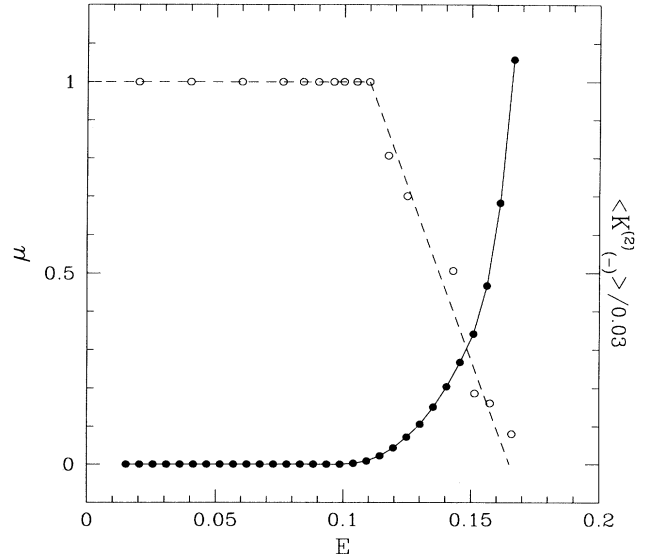

FIG. 8. The absolute values of the integrals of the negative sectional curvature computed for different values of E (full dots) are compared with μ (after Ref. 11), the ratio between the area covered by the regular trajectories and the total area accessible to the motions (open circles).

by a suitable scale factor for graphical reasons (Fig. 8, full dots), it is evident that at the same value of the energy at which μ begins to decrease (i.e., the measure of chaotic trajectories begins to increase), $\langle K_{(-)}^{(2)}\rangle(E)$ starts increasing.

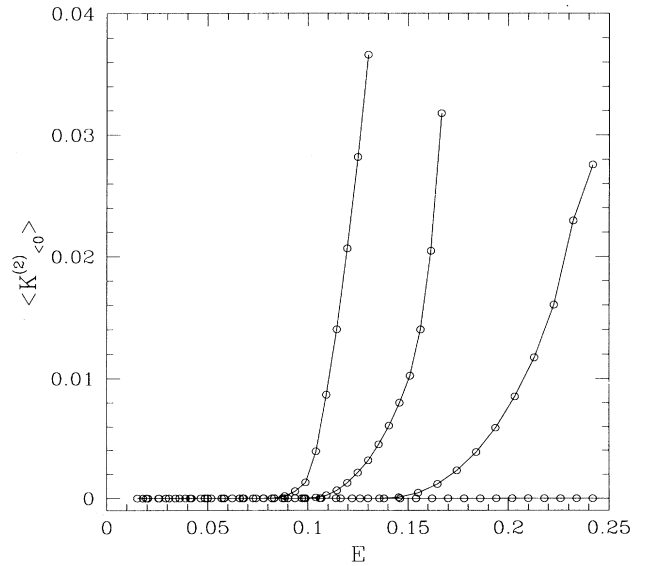We have also computed the fraction of $A(\Sigma_E)$ where

FIG. 9. The absolute value of the integral of the negative sectional curvature is plotted vs the total energy E for different degrees of nonlinearity of the Hénon-Heiles Hamiltonian. From right to left, $\alpha=0.1, 0.85, 1$, and 1.2.

$K^{(2)} < 0$ as a function of E. The transition is again neatly detected. However, $\langle K^{(2)}_{(-)} \rangle$ conveys more information, because it also measures the total degree of instability.

$\langle K^{(2)}_{(-)} \rangle(E)$ has also been obtained at different degrees of nonlinearity. This is controlled by the parameter α introduced into the Hamiltonian function as follows:

$$H = \tfrac{1}{2}(p_1^2 + p_2^2) + \tfrac{1}{2}(q_1^2 + q_2^2) + \alpha(q_1^2 q_2 - \tfrac{1}{3}q_2^3) \qquad (38)$$

($\alpha = 1$ corresponds to the standard HH Hamiltonian). In Fig. 9 we show the behavior of $\langle K^{(2)}_{(-)} \rangle$ plotted vs energy E and computed at different values of α (from right to left, $\alpha = 0.1$, 0.85, 1, and 1.2). It is evident that an increase of the relative weight of the nonlinear part of the potential results, as expected, in a decrease of the threshold energy at which the system makes a transition from a prevailing regular to a prevailing chaotic behavior.

The result of Fig. 8 is very interesting for two reasons: (i) for the first time, to our knowledge the transition from order to chaos is detected in this model in a way that is independent of the dynamics; and (ii) it shows that a geometric stochasticity criterion can actually be found for a two-degrees-of-freedom system. This criterion is not yet in its most general form. In fact, chaotic systems may exist with positive $K^{(2)}$ at any energy and, conversely, the simple choice of $\mathbf{J} \perp \mathbf{v}$ that enters Eq. (36) might give also negative values of $K^{(2)}$ with nonvanishing frequency along regular motions. This suggests that some classification of chaotic systems on geometrical grounds should be possible and is necessary. On the other hand, significant improvements could be achieved by using richer structures than $(M \times \mathbb{R}^2, g_E)$; these could be the configuration-space-time endowed with a Finslerian structure [1], or the already mentioned tangent bundle TM of configuration space equipped with the Sasaki lift of the Jacobi metric.

V. CONCLUSIONS

We have shown that the geometric description of Hamiltonian chaos based on Riemannian geometry is effective, and conveys at least the same qualitative and quantitative information that is provided by the standard phenomenological approaches (Poincaré surfaces of section, Lyapunov exponents). This has been shown for two-degrees-of-freedom Hamiltonians, where the comparison between geometric and conventional descriptions can be performed in great detail. The stability equation used throughout the paper has been derived from the JLC equation without approximations. Therefore, the results reported in the present paper are not simply alternatives to the conventional phenomenological tools to describe chaos, but have a deeper meaning. In fact, the Riemannian approach stems from first principles of classical mechanics, and as it has been shown to give a complete description of the stability properties of the dynamics, it provides an *explanation* of the origin of Hamiltonian chaos which is an alternative to the conventional one based on homoclinic intersections.

We have also put into evidence the main difference between geodesic flows of physics and abstract geodesic flows (Anosov flows). Chaos in physical geodesic flows is mainly due to fluctuations of positive curvature along the geodesics rather than to the hyperbolicity, i.e., to pervasive negative curvature of the ambient manifold.

Finally, we have shown that the order-to-chaos transition in the Hénon-Heiles model can be detected by means of the energy behavior of a geometric quantity which can be computed independently of the dynamics. This is a very interesting and promising result toward a geometric stochasticity criterion of general use for two-degrees-of-freedom Hamiltonians.

[1] M. Pettini, Phys. Rev. E **47**, 828 (1993).

[2] L. Casetti and M. Pettini, Phys. Rev. E **48**, 4320 (1993).

[3] L. Casetti, R. Livi, and M. Pettini, Phys. Rev. Lett. **74**, 375 (1995).

[4] M. Cerruti-Sola and M. Pettini, Phys. Rev. E **51**, 53 (1995).

[5] R. Abraham and J. E. Marsden, *Foundations of Mechanics* (Addison-Wesley, Redwood City, CA, 1987).

[6] T. Levi-Civita, Ann. Math. **97**, 291 (1926).

[7] J. Guckenheimer and P. Holmes, *Nonlinear Oscillations, Dynamical Systems and Bifurcations of Vector Fields* (Springer-Verlag, Berlin, 1983).

[8] A. J. Lichtenberg and M. A. Lieberman, *Regular and Chaotic Dynamics* (Springer-Verlag, Berlin, 1992).

[9] A. H. Nayfeh and D. T. Mook, *Nonlinear Oscillations* (Wiley, New York, 1979).

[10] H. T. Davis, *Introduction to Nonlinear Differential and Integral Equations* (Dover, New York, 1962), p. 59.

[11] H. Hénon and C. Heiles, Astron. J. **69**, 73 (1964).

[12] Y. F. Cheng, M. Tabor, and J. Weiss, J. Math. Phys. **23**, 531 (1982).

[13] Precisely, a positive measure of points where $K^{(2)} < 0$ could be not sufficient to make unstable the solutions of Eq. (31). In fact it is well known that a reversed pendulum can be stabilized by a sufficiently rapidly varying force term. This is described by the equation $\ddot{x} + (\omega^2 \pm d^2)x = 0$, where $\omega^2 \pm d^2$ is alternatively positive and negative [see V. I. Arnold, *Les Méthodes Mathématiques de la Méchanique Classique* (MIR, Moscow, 1976)]. In any case this is a very special exception.

[14] L. P. Eisenhart, Ann. Math. **30**, 591 (1929).

[15] W. Klingenberg, *Riemannian Geometry* (de Gruyter, Berlin, 1982).